



Cite this: DOI: 10.1039/d5lc00586h

## sNails: sweat-sensing nails for unobtrusive, wearable microfluidic sweat monitoring from the dorsal distal phalanges

Noelle Davis, <sup>a</sup> Pooja Mehta, <sup>b</sup> Amanda Kang, <sup>b</sup> Liam Gillan, <sup>c</sup> Jussi Hiltunen <sup>d</sup> and Ali Javey <sup>\*ae</sup>

We present a fingernail-mounted microfluidic sweat sensor, the sNail, that leverages the anatomical and mechanical advantages of the nail plate and adjacent dorsal finger skin—regions that are uniquely stiff and stable yet underutilized for wearable biosensing. In contrast to fully soft, skin-mounted sensors, our device exploits the rigidity of the nail to host microfluidics that remain stable under typical daily finger motion. The platform incorporates a hydrogel-filled sweat collection well and stretchable thermoplastic polyurethane (TPU) microfluidics, fabricated *via* scalable laserjet printing and laser cutting. We demonstrate frequent sweat rate monitoring across multiple fingers and subjects during activities ranging from walking to typing, and capture dynamic changes in sweat rate associated with both physical exertion and psychological stress. This nail-mounted approach enables unobtrusive, informative sweat biosensing, paving the way for broader adoption in everyday settings.

Received 13th June 2025,  
Accepted 10th September 2025

DOI: 10.1039/d5lc00586h

rsc.li/loc

### I. Introduction

Amid the growing trend towards soft, stretchable, electronics for on-skin wear, we design the Sweat-Sensing Nail, or sNail: a wearable sweat sensor device for mounting on the nail plate and adjacent strip of skin—both uniquely stiff and stable surfaces of the body. Together, these regions provide an ideal base for a robust, unobtrusive sweat sensor with future potential for easy integration of powerful, rigid silicon electronics.

The dorsal distal phalange of the finger has two unique features. First, it has a notable absence of soft musculoskeletal tissues, minimizing sensor susceptibility to motion artifacts, and secondly, contains the stiff, immobile surface of the nail plate. Except for the thumb, the fingers contain no muscular tissue, relying instead on muscles in the hand and forearm. Additionally, tendons and ligaments in the fingers terminate at the distal interphalangeal joint—the outermost knuckle.<sup>1</sup> Beyond that, the skin sits only on a thin layer of fatty tissue over the bone, resulting in a highly stable surface for sensor placement. The adjacent nail plate is also unique, composed of

the fibrous protein keratin with a typical thickness of 0.5 mm and surface area on the order of 0.5–2 cm<sup>2</sup>.<sup>2</sup> It grows from the fingernail matrix, which is embedded below and behind the nail plate and visible as the whitish arc at the base of the nail, at a rate of a few millimeters per month.<sup>2,3</sup> The fibers of the top and bottom layer of the nail are oriented in the direction of nail growth, whereas the central layer has perpendicular fibers. The effective Young's modulus of this three-layer structure is about 2.9 GPa,<sup>4</sup> representing a stiffness similar to acrylic. Further, the fingernails experience relatively low stress while completing day-to-day tasks. For example, the overall average peak reaction force measured during typing was 2.54 N,<sup>5</sup> and assuming a nail area of 0.5 cm<sup>2</sup> gives a stress of 0.05 MPa. Thus, the nail experiences relatively low levels of deformation, making it highly suitable for mounting strain-sensitive devices. In fact, mounting rigid plates on top of the nail is already a common aesthetic practice, such as decorative acrylic nail extensions. The stability of this skin site and adjacent nail plate makes it an ideal candidate for biosensor placement.

Most academic and commercial sweat sensors to date have been developed for use on the arm or other large-area skin sites during physical activity,<sup>6–8</sup> but recently, several have targeted the fingertip at rest, taking advantage of its relatively high sweat rate.<sup>9</sup> This development is promising because sweat has been shown to reflect a range of physiological processes—not only hydration during exercise and high temperatures, but also everyday biomarkers such as hormone levels and drug dosage, including circadian cortisol rhythms<sup>10,11</sup> and caffeine metabolism.<sup>12,13</sup> Palms and fingers

<sup>a</sup>Department of Electrical Engineering and Computer Sciences, University of California, Berkeley, California, USA

<sup>b</sup>Department of Bioengineering, University of California, Berkeley, California, USA

<sup>c</sup>VTT Technical Research Centre of Finland, Espoo, Finland

<sup>d</sup>VTT Technical Research Centre of Finland, Oulu, Finland

<sup>e</sup>Materials Sciences Division, Lawrence Berkeley National Laboratory, Department of Electrical Engineering and Computer Sciences, University of California, Berkeley, California, USA. E-mail: ajavey@berkeley.edu

are widely recognized to have a particularly high sweating rate among bodily skin sites. While most rigorous body mappings of sweat rate have been conducted during heat stress from exercise or elevated environmental temperatures in part due to lack of precise sweat rate sensors,<sup>14,15</sup> they show that the hands exhibit a relatively high baseline sweat rate, higher than that of the arms, and experience less extreme increases during exercise compared to regions such as the back.<sup>15</sup> This elevated yet stable sweat rate is well-suited for continuous sweat collection without quickly saturating a sensor's capacity.

Taking advantage of this are palmar fingertip sensors of two varieties: for the benchtop<sup>10,16–18</sup> and, fewer in number, for on-body wear.<sup>9,19–21</sup> Unobtrusive wearable sensors on high sweat-rate sites could enable continuous noninvasive biosensing in ways not previously possible. Especially with the use of microfluidics, which isolate sweat from the surrounding environment, sensors can function reliably in a variety of conditions including high heat, humidity, and even aquatic settings.<sup>22,23</sup> In addition to their high sample rate, however, the palmar fingertips are a high-contact skin site where a wearable sensor would be significantly disruptive to daily life, *e.g.* typing, grasping objects, *etc.* Alternatively, the skin on the dorsal side of the finger—between fingernail and knuckle—experiences much less contact during routine activities but still exhibits a notably high sweat rate. One study measured over 70% the sweat rate of the palmar fingertip at this site across multiple subjects at rest and during exercise.<sup>24</sup> Further, a device capable of sampling from this skin site could utilize the adjacent rigid surface of the nail plate to mount connected microfluidics, with minimal artifacts from motion or activity involving the fingers, as shown in this work. In future work, the nail plate could also mount silicon electronics for electrochemical interrogation of sweat rate and chemical contents.

## II. Experimental

### Laserjet printing of TPU film

First, TPU (Covestro AG Platilon U073, 100  $\mu\text{m}$  thickness) was roll-to-roll (R2R) laminated with a polyethylene terephthalate (PET) carrier foil (DuPont Melinex ST506, 75  $\mu\text{m}$  thickness) and thermally treated (140 °C oven, dwell time ~3.5 min). This was additionally laid on top of a sheet of cardstock paper to be fed into an HP LaserJet 1022 printer. Designs were printed at a resolution of 1200 dpi. Designs were created as vector drawings in AutoCAD and assigned a line width of 0.09 mm for printing.

### Laser cutting of films

Four separate layers were laser cut: (1) printed TPU film, (2) microfluidic spacer (3) skin-side adhesive, as well as (4) hydrogel mold. Polyester film with double-sided acrylate adhesive was used for the microfluidic spacer, skin-side adhesive, and upper layer of hydrogel mold. All laser cutting was done with a Universal Laser Systems PLS4.75 CO<sub>2</sub> laser

equipped with a BOFA AD 1000 iQ fume extractor. Before cutting, each film was stretched taut on a backing sheet of  $\frac{1}{4}$ " acrylic with scotch tape, and the laser z-axis was aligned to the material surface. All cuts were done at highest vector resolution and 1000 ppi as set by the accompanying Universal Control Panel software, with power and speed tuned for each material. The TPU with carrier foil was laser cut at 3.0% power and 6% speed, and after completion of cutting the fumes were ventilated for at least 10 seconds to clear the headspace before opening the laser bed. The microfluidic spacer was cut at 2.1% power and 6% speed. For the backing and skin-side adhesive layer, one side of the material was stripped of its acrylate adhesive using isopropyl alcohol to serve as the floor of the microfluidic channel. The remaining material was then cut at 1.8% power and 6% speed along the perimeter, and at 3.2% power and 6% speed around the collection well to remove the back liner for hydrogel insertion. Finally, the upper layer of the hydrogel mold was cut at 3.2% power and 6% speed (Fig. 1).

### Fabrication of hydrogel collection medium

The hydrogel mold was assembled by laminating the laser-cut upper layer onto a sheet of hydrophilic PET (3M 9984).

To prepare the hydrogel, 0.1 g of agarose, 2.5 mL of glycerol, 1 mL deionized water, and 7 drops of food dye were vortexed to mix before heating at 120 °C with continuous stirring. After dissolution over 5 minutes of heating, 2.8  $\mu\text{L}$  of hydrogel solution was pipetted into each well of the laser cut mold, with temperature reduced to 80 °C and held there to maintain low solution viscosity, and then hydrogels cured at room temperature for 36 hours prior to use (Fig. 2g).

### Device assembly

For assembly, the spacer layer (3M 9965) had its channel material removed, the TPU film was laminated on top, and then this stack was laminated onto the skin-side adhesive. For adhesion strength, pressure was applied with a handheld roller followed by annealing at 130 °C under a weight for each lamination step. Finally, hydrogel was transferred into the collection well, and the opening in the carrier film was sealed with tape for storage.

### Human subject studies

The nail plate and adjacent strip of skin were first wiped with an alcohol swab. Then, a device was taken from the sheet, trimmed to fit the length of the individual nail as needed, and then adhered to the finger with the collection well positioned below the cuticle and above the knuckle. Throughout the experiment, periodic smartphone photographs were taken with a clear view of the sweat progressing through the channel.

Subject heart rate and environmental temperature and relative humidity were monitored alongside sweat rate for some experiments using a Fitbit smartwatch and Govee H5075 Thermometer.

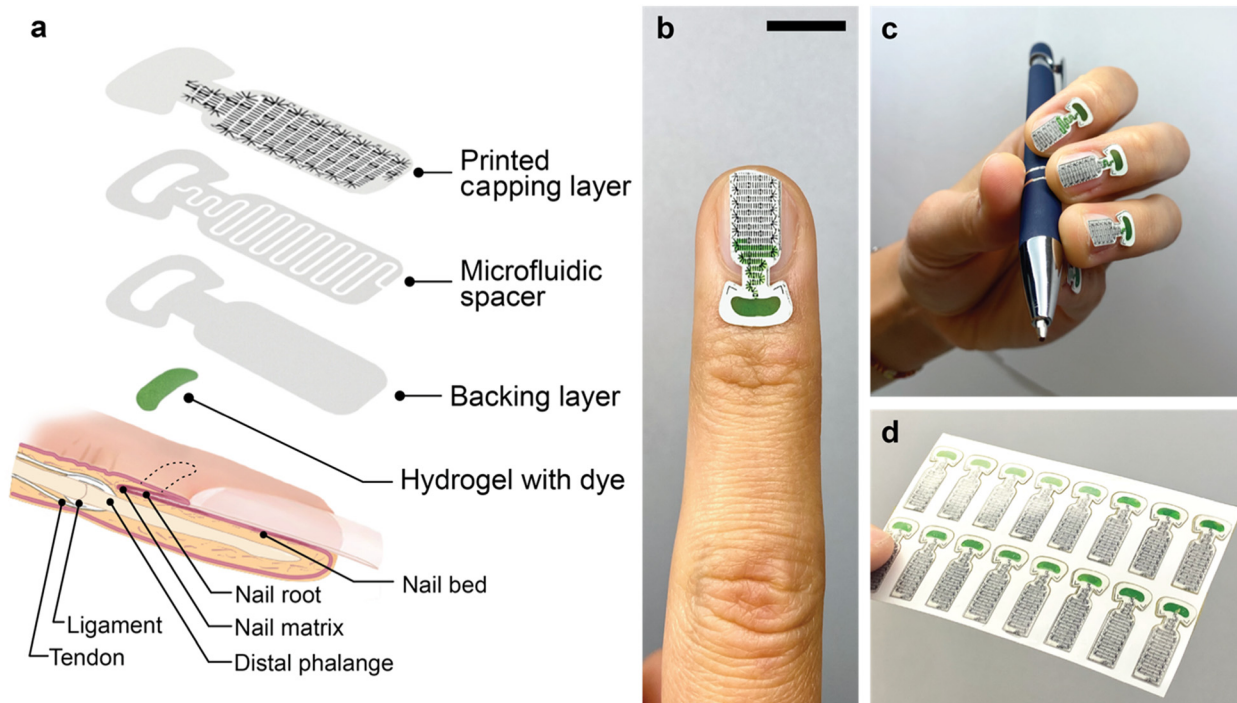


**Fig. 1** sNail fingernail-mounted sweat sensing platform. (a) Exploded schematic of the multilayer device architecture: printed TPU capping layer, microfluidic spacer, backing layer with skin adhesive, and molded hydrogel skin interface aligned over the distal phalanx. Anatomic illustration shows placement relative to the nail bed and sweat gland-rich fingertip skin. (b) Photograph of the device adhered to the dorsal finger skin and fingernail, conforming to its curvature. (c) Demonstration of the device worn on four fingers during use of the hand (e.g., holding a pen), illustrating minimal disruption to dexterity. (d) Sheet of fully assembled sensors prior to application, highlighting batch fabrication and scalability. Scale bar: 1 cm.

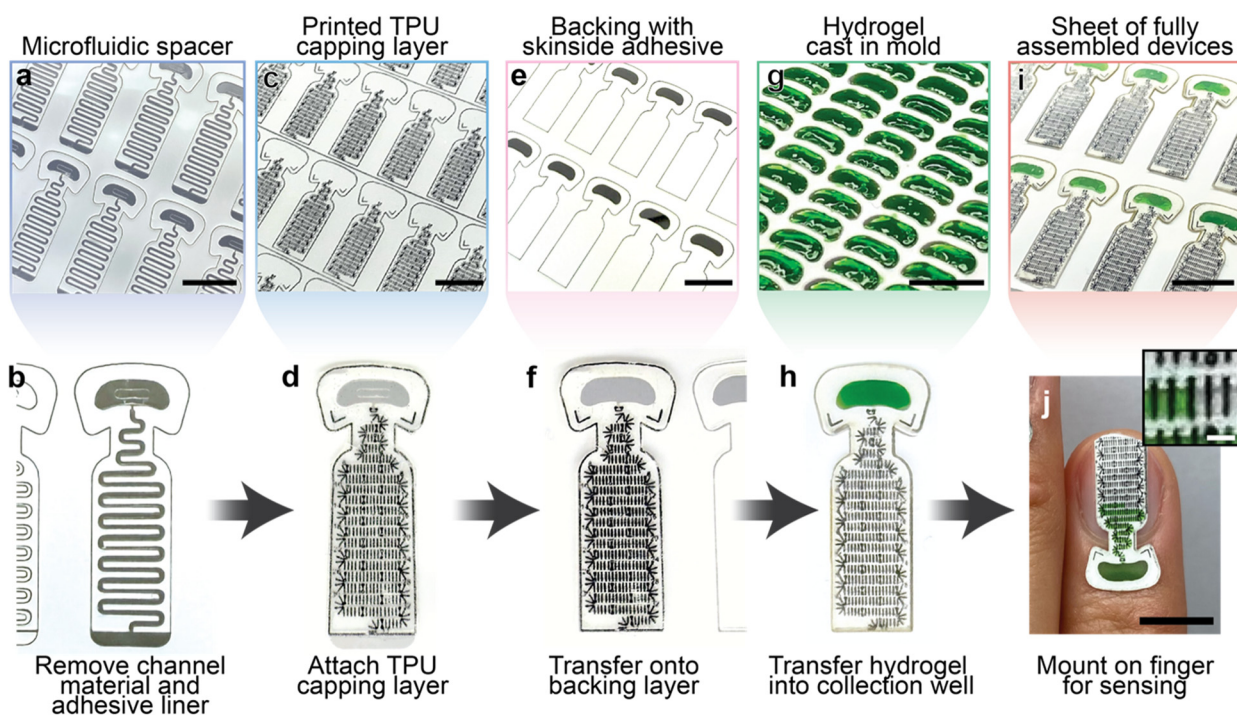


**Fig. 2** Scalable assembly of the nail-mounted microfluidic sweat sensors. (a-j) Step-by-step fabrication and integration process: (a) laser cutting of the microfluidic channel layer and (b) preparation of a single device; (c) laser-jet printing of the capping layer and (d) adhesion to a microfluidic spacer; (e) laser cutting of the backing layer with skin-side adhesive and (f) transfer of fluidic onto the backing layer; (g) hydrogel casting into separate mold and (h) hydrogel transfer into a device; (i) sheet of fully assembled devices and (j) device applied on the finger with inset showing the fluid front for optical readout of sweat volume. The process supports batch production for easy and low-cost device fabrication as well as consistent performance. Scale bars: 1 cm except for inset of (j) which is 100  $\mu$ m.

On-body human trials were carried out at the University of California, Berkeley in compliance with human research protocol (CPHS 2014-08-6636) approved by the Berkeley Institutional Review Board (IRB) and U.S. federal regulations on human subjects in research (Title 45, Part 46, Code of Federal Regulations), as well as at VTT in compliance with protocol approved by the VTT Research Ethics Committee. All experiments were performed in accordance with the Declaration of Helsinki. Informed consent was obtained from all participants of this study.

### Data processing

Upon the completion of an experiment, the number of gates up to the fluid front was counted in each image with the help of printed markers indicating ten gate intervals. Then, these data were compiled to report the average sweat rate between each image, taking the change in sweat volume between images divided by the time interval and normalizing by the area of the collection well. Average sweat rates for the time periods between images are plotted alongside subject heart rate and environmental temperature to produce the results shown in Fig. 5.

## III. Results and discussion

### Design of an unobtrusive microfluidic sweat sensor on the dorsal distal phalange

A uniquely secure and stable surface for sweat sensor attachment exists on the skin of the finger between the nail plate and distal interphalangeal joint, or furthest knuckle. We will first discuss the design of a sweat collector for this skin surface, and second, the design of microfluidic sweat rate measurement channels for the adjacent nail plate. In this area of the finger, the skin lies directly above the distal phalanx bone, with minimal soft tissue in between. Notably, the fingers contain no muscles, aside from the thumb, with their movement instead driven by muscles in the hand and forearm. Additionally, ligaments and tendons terminate at the base of the distal phalanx bone, so that the region of skin beyond the joint experiences minimal deformation from stretching and compression during typical hand movements.

With this anatomical context in mind, we designed an oblong sweat collection well for the sNail that traces the curve of the cuticle and sits in front of the knuckle, measuring 5.7 mm wide and 2.2 mm long, enclosing an area of  $10\text{ mm}^2$  (Fig. 1). The collection well is surrounded and sealed by a strip of adhesive, 1.2 mm wide at its narrowest, directing sweat into the microfluidic channel without leakage or evaporative loss. Within the collection well, a hydrogel interface—approximately 100  $\mu\text{m}$  thick and molded to precisely fill the well—facilitates sweat uptake from the skin and enables optical readout through sample coloration. As described in previous work,<sup>9</sup> the hydrogel interface permits sizing of the collection well to access a sufficient number of sweat glands for adequate sample volume while minimizing dead volume. Among several fabrication methods tested,

including large-area casting and stamping, in-device casting and curing, and mold casting for transfer, the mold casting method provided the most control over hydrogel volume and shape. Large-area casting suffered from variation in thickness, and in-device casting led to unwanted seepage into the channel. In contrast, mold casting enabled controlled dispensing of solution volume with consistent shape for each device.

The microfluidic channel in the sNail serves to quantify the collected sweat volume, and in future iterations could also accommodate electrochemical sensors for time-resolved measurements of sweat biomarkers. Three channel variations were designed, as detailed in Table S1. The first is a high-capacity serpentine channel with width of 450  $\mu\text{m}$  and length of 87 mm within a 17 mm device footprint, yielding a volumetric capacity of 3.4  $\mu\text{L}$ . Additionally, two straight channel designs were developed to facilitate data processing, with widths of 450  $\mu\text{m}$  and 750  $\mu\text{m}$  providing capacities of 0.7  $\mu\text{L}$  and 1.1  $\mu\text{L}$ . To enable optical readout of sample volume, linear reference markings were printed along the length of the channel on the capping layer. In the serpentine design, printed reference markers indicate 10 nL increments, and in the narrow and wide linear designs, increments of 10 nL and 16 nL, respectively.

The device materials were selected for their pliability, fluid resistance, and compatibility with scalable processing. Building on a layer stack developed in previous work,<sup>25–27</sup> stiffer PET films were replaced with soft, stretchable TPU on the top of the microfluidic channel and combined with skin-side adhesive layer on the bottom of the channel. These material choices allow the device to better conform to the finger's curvature without pulling away from the skin during prolonged wear during a range of daily activities. A fluid-impermeable polyester film with double-sided acrylate adhesive was used for both the microfluidic spacer and the backing layer with skin-side adhesive. Images of the laser-cut layers and assembly process are shown in Fig. 2.

### Characterization of microfluidic during extreme finger movements in on-body wear

To test its robustness, the sNail was challenged with extreme finger movements as well as water exposure. As shown in Fig. 3 and S2, subjects performed multiple cycles of each test condition with a device mounted on their index finger. First, the subject flexed the finger and returned it to a resting position ten times, with the device imaged at both flexion and rest for each cycle. Next, they hyperextended their finger by pressing the fingertip against a hard surface and then returning to rest, also ten times. Finally, they washed their hands under running tap water for thirty seconds, followed by removal from the water for imaging, repeated for three cycles. In all cases, fluid progression within the microfluidic channel remained consistent, indicating that sweat rate was unaffected by finger movement or water exposure.

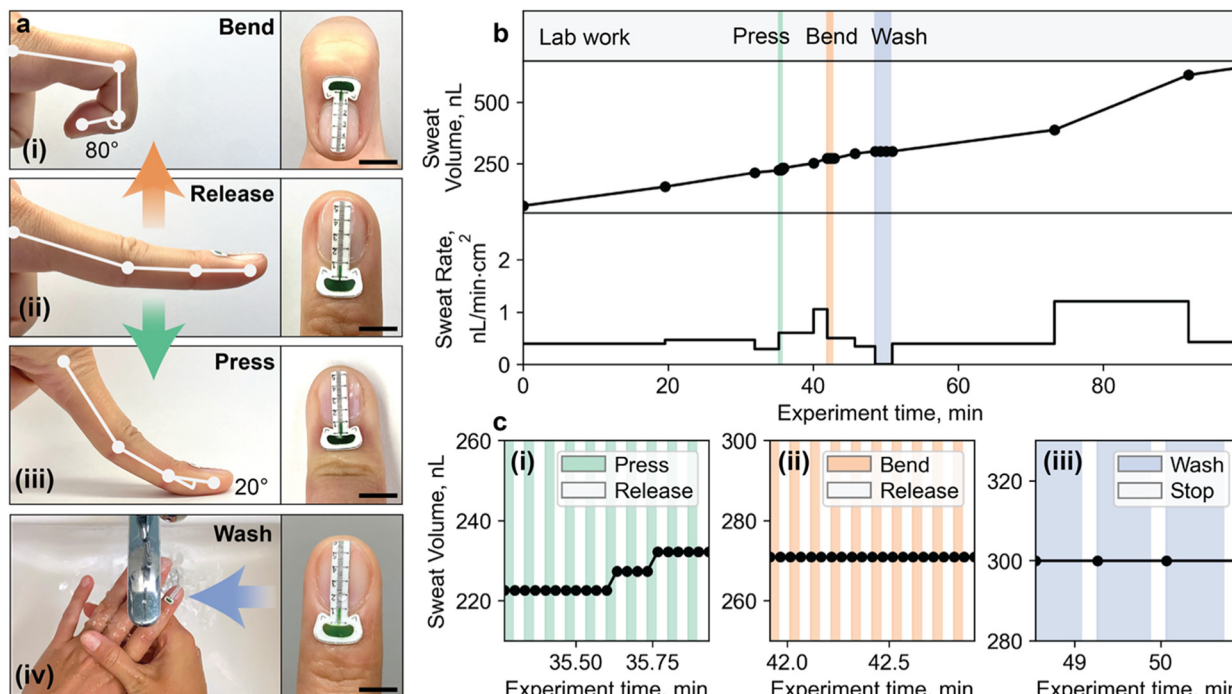


**Fig. 3** Device performance on the index finger during mechanical and environmental stress tests. (a) Photographs of representative finger motions, each of which repeated in multiple cycles during the experiment: (i) finger bending, (ii) return to rest, (iii) fingertip pressing against a surface, and (iv) hand washing under running water. (b) Total collected sweat volume and calculated sweat rate over the course of the experiment, segmented by activity phase: baseline, pressing cycles, bending cycles, and hand washing cycles. (c) Expanded views of sweat volume measured during (i) 10× cycles of press and release, (ii) 10× cycles of bend and release, and (iii) 3× cycles of hand washing and subsequent removal. The stable signal throughout motion and water exposure indicates robust and continuous sweat collection with minimal disruption. Scale bars: 1 cm.

### Assessing the suitability of different fingers for sweat sample collection

Several experiments were conducted to assess the suitability of each finger for continuous sweat collection. The thumb was excluded from these tests due to pumping of fluid inside the channel being observed during flexion and extension, which might be attributed to this finger's unique musculature, as the only finger containing muscle tissue. As shown in Fig. 4, experiments were carried out among three different subjects, including typical daily activities such as walking, office work involving a mouse and/or keyboard, and lab work involving use of the hands. Sweat volumes were calculated from the moment fluid entered the channel of the last sNail, until either the end of the experiment or the point when the first sNail's channel was completely filled. Across the subjects, the index and pinky fingers showed the highest sweating rates, followed by the middle finger. The ring finger sweat rate was much lower, possibly related to its unique divided innervation<sup>28</sup> (Fig. 4a). Across individual measurements, there was some variation in the ratios between index and each other fingers for each subject, some of which could be attributed to different activities and environmental conditions (Fig. 4b). The particularly high variation for the pinky could be caused by pumping effects in the fluidic, with its higher curvature and smaller surface area before the knuckle. On the forearm, even some negative flow rates were observed, representing backwards flow in the

microfluidic channel and reabsorption into the skin under very low sweat rates. However, overall, every finger expressed a higher sweat rate than that of the forearm, demonstrating their better suitability as sites for continuous sweat collection.

### Sensing fingertip sweat on-body during typical daily activities

Further experiments measured the sweat rate across fingers as a time-series during various activities, with subjects wearing sNails on four fingers as well as and in some cases the arm (Fig. 5). The first experiment involved subjects #1 and #2 taking a walk together. In the same temperature and humidity conditions and same activity, as well as similar heart rates, there is of course individual variation in sweating rate. During light walking, the sweat rate clearly rises across all four fingers, up to  $8 \text{ nL min}^{-1} \text{ cm}^{-1}$  for subject #1 and  $4 \text{ nL min}^{-1} \text{ cm}^{-1}$  for subject #2. Similar dynamic trends are observed for each finger. In the second experiment, also involving light walking, the sweat rate for subject #1 can be compared with subject #3, who has a  $5 \text{ nL min}^{-1} \text{ cm}^{-1}$  spike during walking. Finally, during a time-constrained typing game to induce psychological stress, subject #2 experiences elevated sweat rates on the index and pinky fingers, with no such sensitivity on the arm.

In contrast to the high sweat rates induced by exercise or elevated temperature, endogenous sweating presents an opportunity to monitor subtle sweat rate variations in response

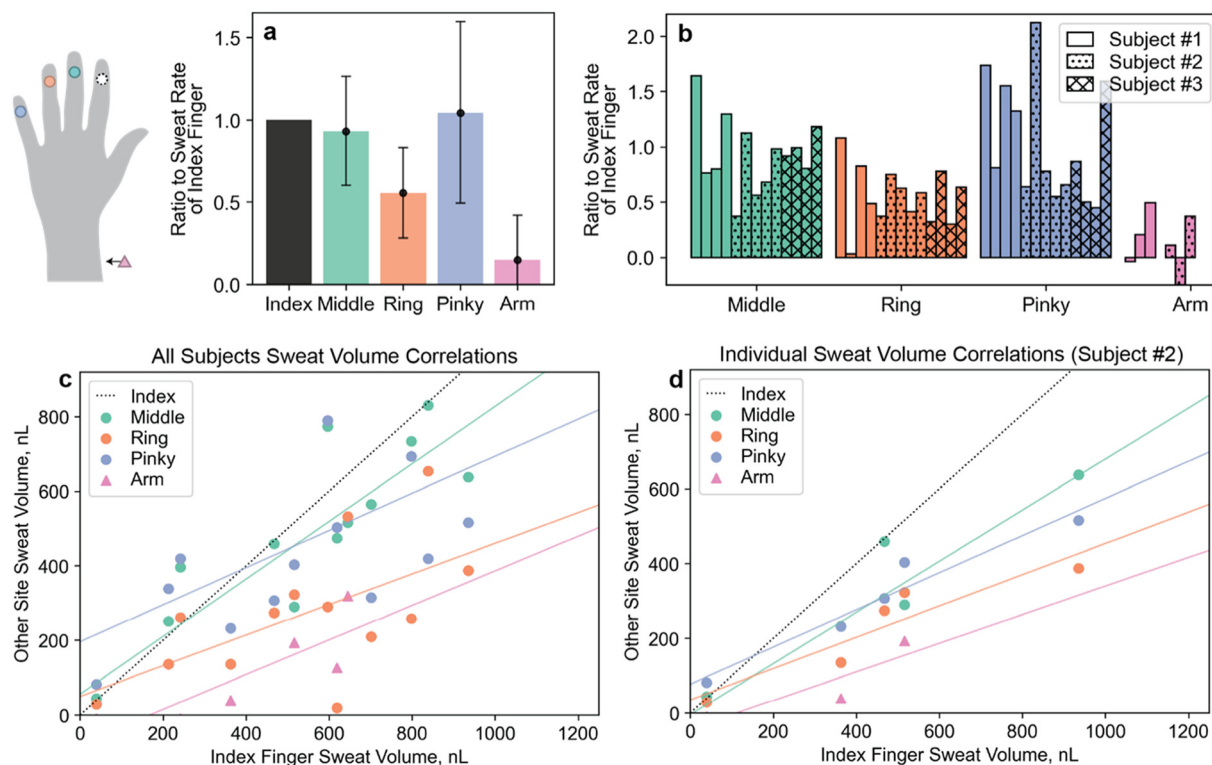


**Fig. 4** Comparison of sweat secretion rates across four fingers and the arm across three subjects during various activities in multiple experiments. (a) Mean and standard deviation of sweat rates for different fingers and the volar forearm, normalized to the index finger. (b) Individual subject data showing variation in sweat rate ratios relative to the index finger across different experiments. (c) Pooled subject data showing correlation between sweat volume collected at the index finger and other sites (middle, ring, pinky, and volar forearm). (d) Individual-level correlation (subject #2 shown) between index finger sweat volume and volumes from other sites. Data illustrate consistent inter-site relationships on the individual level and support the index, middle, and pinky fingers as good choices for a high-yield sampling location.

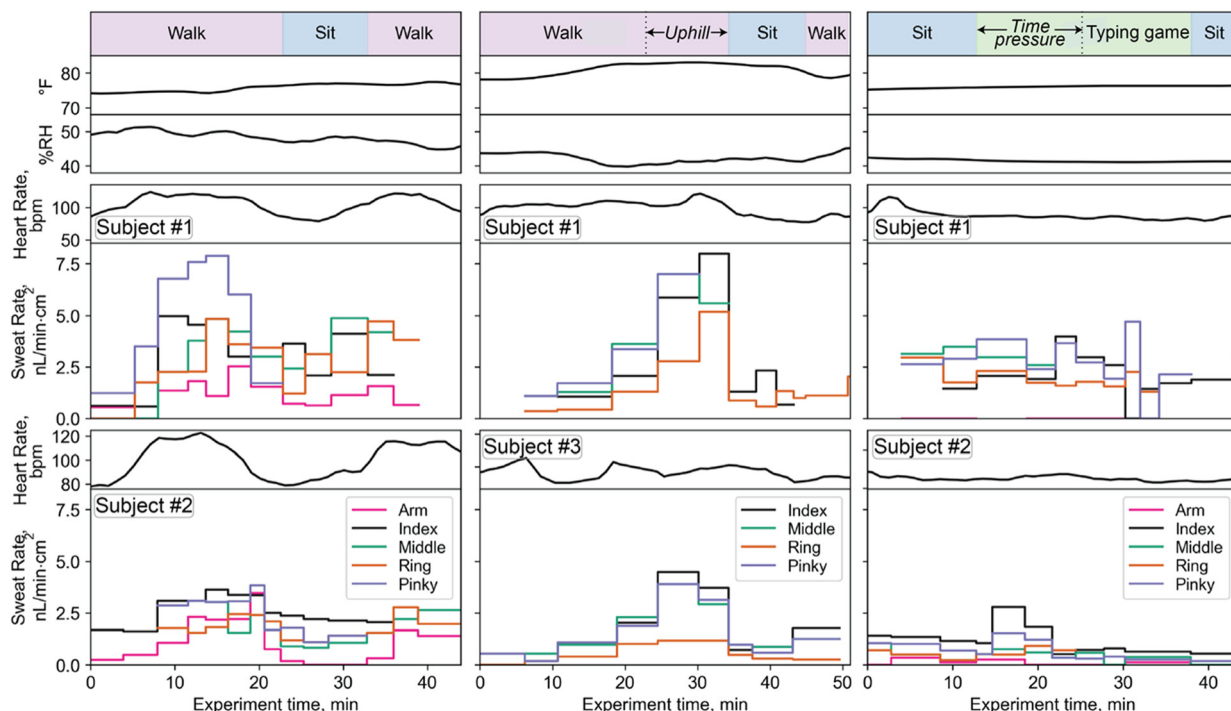


**Fig. 5** Sweat monitoring on four fingers and the arm for multiple subjects during regular daily activities including walking, seated rest and work, and typing under pressure. Sweat rates are elevated during periods of physical activity and typing under pressure. Ambient temperature and relative humidity during the three experiments ranged from 74–84 °F and 39–52%.

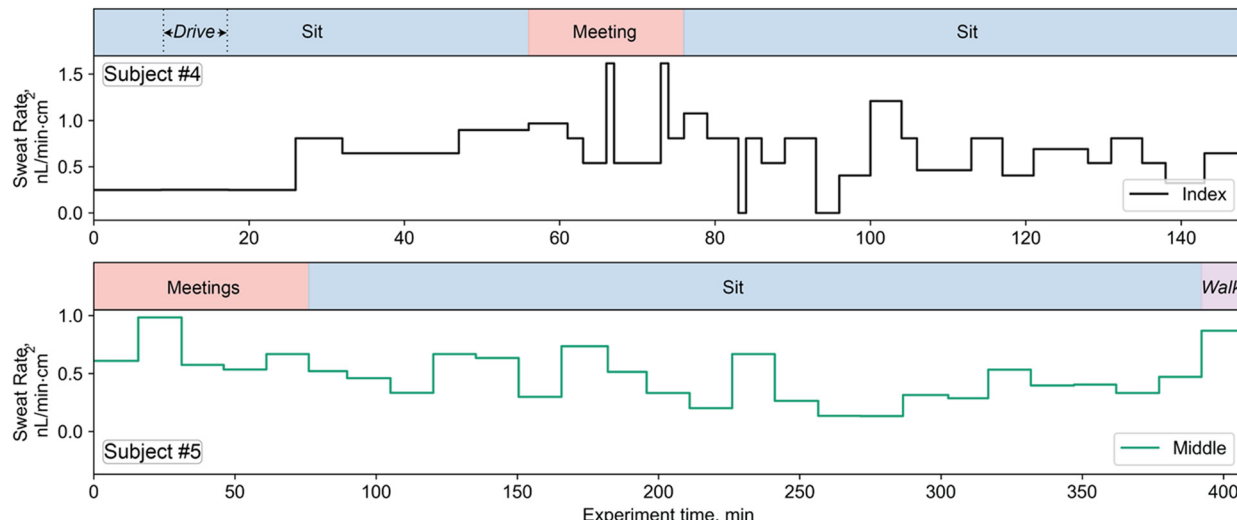


**Fig. 6** Long-term sweat monitoring on the index or middle finger with periods of meetings between seated work. Elevated sweat rates reflect possible psychological stress experienced during the meetings.

to induced cognitive stress. In an earlier study we observed that by measuring changes in sweat rate from a sensor mounted on the fingertip it is possible to identify stress state triggered by public speaking events.<sup>9</sup> Fig. 6a presents a measurement from the left index finger of a subject who drove a car for around five minutes during a period between the first two data points, before performing seated computer work for the remainder of the trial. This computer work included a video meeting with colleagues. The subject did not consider the meeting to be a stressful event. Despite the subject's reported lack of stress, during the meeting the sweat rate increased above the baseline level to  $1.5 \text{ nL min}^{-1} \text{ cm}^{-1}$ . This suggests that the subject may have experienced elevated stress levels during the meeting even though they were not aware of this. Fig. 6b presents another subject doing seated work with meetings, where sweat rate is elevated during the meetings as well. This type of sensor could be employed in future work for a systematic study into correlations between endogenous sweating and cognitive stress.

## IV. Conclusion

The sNail, a wearable sweat sensor device for the dorsal side of the finger, presents the opportunity for continuous, noninvasive biosensing, taking advantage of the high sweat rate of the fingers and the rigid surface of the fingernail. Results from subject studies demonstrate the sensitivity of the device to a wide range of activities. For at-rest or near-rest activities, sweat rates were higher for every finger compared to the forearm. A stress-inducing activity saw elevated sweat rates on certain fingers compared to no sensitivity on the forearm. The use of inexpensive, unobtrusive microfluidic devices with higher sensitivity opens the possibility for continuous sweat rate monitoring during routine activities and over long periods of time. Future work could explore the potential of integrating electronics to automate measurements of fluid flow and electrochemical sensors for detailed sweat analysis.

## Conflicts of interest

There are no conflicts to declare.

## Data availability

Supplementary information is available, including further details on and characterization of the microfluidic device. See DOI: <https://doi.org/10.1039/D5LC00586H>.

The data supporting the findings of the study are included in the manuscript and SI. Raw data can be obtained from the corresponding author upon request.

## Acknowledgements

This work was supported by the Berkeley Sensors and Actuators Center (BSAC), and the work at VTT by the Research Council of Finland (grants 351282 and 358621) and EU (Ultrasense project, grant 101130192). We thank Pekka Ontero for technical assistance in R2R TPU preparation, as well Tess Despres for proposing the name of the device. N. D. acknowledges support from the National Defense Science and Engineering Graduate (NDSEG) Fellowship Program, and A.K. acknowledges support from the Bakar Ignite Scholars Program.

## References

- 1 R. Schwarz and C. Taylor, The Anatomy and Mechanics of the Human Hand, *Artif. Limbs*, 1955, 2(2), 22–35.
- 2 J. W. H. Mali, *Some Fundamental Approaches in Skin Research*, Karger Medical and Scientific Publishers, 1981.
- 3 S. Yaemsiri, N. Hou, M. Slining and K. He, Growth Rate of Human Fingernails and Toenails in Healthy American Young Adults, *J. Eur. Acad. Dermatol. Venereol.*, 2010, 24(4), 420–423, DOI: [10.1111/j.1468-3083.2009.03426.x](https://doi.org/10.1111/j.1468-3083.2009.03426.x).

- 4 H. Tohmyoh and M. Abukawa, Nanoindentation Study of Human Fingernail for Determining Its Structural Elasticity, *Sking Res. Technol.*, 2023, **29**(10), e13456, DOI: [10.1111/srt.13456](https://doi.org/10.1111/srt.13456).
- 5 B. J. Martin, T. J. Armstrong, J. A. Foulke, S. Natarajan, E. Klinenberg, E. Serina and D. Rempel, Keyboard Reaction Force and Finger Flexor Electromyograms during Computer Keyboard Work, *Hum. Factors*, 1996, **38**(4), 654–664, DOI: [10.1518/001872096778827288](https://doi.org/10.1518/001872096778827288).
- 6 J. Choi, D. Kang, S. Han, S. B. Kim and J. A. Rogers, Thin, Soft, Skin-Mounted Microfluidic Networks with Capillary Bursting Valves for Chrono-Sampling of Sweat, *Adv. Healthcare Mater.*, 2017, **6**(5), 1601355, DOI: [10.1002/adhm.201601355](https://doi.org/10.1002/adhm.201601355).
- 7 L. B. Baker and A. S. Wolfe, Gx Sweat Patch and App for Personalized Hydration, *Sports Science Exchange*, 2022, **35**(234), 1–8.
- 8 N. Mishra, N. T. Garland, K. A. Hewett, M. Shamsi, M. D. Dickey and A. J. Bandodkar, A Soft Wearable Microfluidic Patch with Finger-Actuated Pumps and Valves for On-Demand, Longitudinal, and Multianalyte Sweat Sensing, *ACS Sens.*, 2022, **7**(10), 3169–3180, DOI: [10.1021/acssensors.2c01669](https://doi.org/10.1021/acssensors.2c01669).
- 9 H. Y. Y. Nyein, M. Bariya, B. Tran, C. H. Ahn, B. J. Brown, W. Ji, N. Davis and A. Javey, A Wearable Patch for Continuous Analysis of Thermoregulatory Sweat at Rest, *Nat. Commun.*, 2021, **12**(1), 1823, DOI: [10.1038/s41467-021-22109-z](https://doi.org/10.1038/s41467-021-22109-z).
- 10 W. Tang, L. Yin, J. R. Sempionatto, J.-M. Moon, H. Teymourian and J. Wang, Touch-Based Stressless Cortisol Sensing, *Adv. Mater.*, 2021, **33**(18), 2008465, DOI: [10.1002/adma.202008465](https://doi.org/10.1002/adma.202008465).
- 11 N. I. Hossain, T. Noushin and S. Tabassum, StressFit: A Hybrid Wearable Physicochemical Sensor Suite for Simultaneously Measuring Electromyogram and Sweat Cortisol, *Sci. Rep.*, 2024, **14**(1), 29667, DOI: [10.1038/s41598-024-81042-5](https://doi.org/10.1038/s41598-024-81042-5).
- 12 L.-C. Tai, W. Gao, M. Chao, M. Bariya, Q. P. Ngo, Z. Shahpar, H. Y. Y. Nyein, H. Park, J. Sun, Y. Jung, E. Wu, H. M. Fahad, D.-H. Lien, H. Ota, G. Cho and A. Javey, Methylxanthine Drug Monitoring with Wearable Sweat Sensors, *Adv. Mater.*, 2018, **30**(23), 1707442, DOI: [10.1002/adma.201707442](https://doi.org/10.1002/adma.201707442).
- 13 M. Su, L. Zhu, Y. Zhou, Z. Ding, Y. Yao, M. Li, Q. Qiu, W. Peng, H. Gao and C. Yu, Wearable Biosensing of Caffeine via Microfluidic-Integrated Agarose Hydrogels for Personalized Metabolic Monitoring, *Anal. Chem.*, 2025, **97**(29), 15835–15843, DOI: [10.1021/acs.analchem.5c01954](https://doi.org/10.1021/acs.analchem.5c01954).
- 14 C. J. Smith and G. Havenith, Body Mapping of Sweating Patterns in Male Athletes in Mild Exercise-Induced Hyperthermia, *Eur. J. Appl. Physiol.*, 2011, **111**(7), 1391–1404, DOI: [10.1007/s00421-010-1744-8](https://doi.org/10.1007/s00421-010-1744-8).
- 15 N. A. Coull, A. M. West, S. G. Hodder, P. Wheeler and G. Havenith, Body Mapping of Regional Sweat Distribution in Young and Older Males, *Eur. J. Appl. Physiol.*, 2021, **121**(1), 109–125, DOI: [10.1007/s00421-020-04503-5](https://doi.org/10.1007/s00421-020-04503-5).
- 16 S. Lin, B. Wang, Y. Zhao, R. Shih, X. Cheng, W. Yu, H. Hojaiji, H. Lin, C. Hoffman, D. Ly, J. Tan, Y. Chen, D. Di Carlo, C. Milla and S. Emaminejad, Natural Perspiration Sampling and in Situ Electrochemical Analysis with Hydrogel Micropatches for User-Identifiable and Wireless Chemo/Biosensing, *ACS Sens.*, 2020, **5**(1), 93–102, DOI: [10.1021/acssensors.9b01727](https://doi.org/10.1021/acssensors.9b01727).
- 17 J. R. Sempionatto, J.-M. Moon and J. Wang, Touch-Based Fingertip Blood-Free Reliable Glucose Monitoring: Personalized Data Processing for Predicting Blood Glucose Concentrations, *ACS Sens.*, 2021, **6**(5), 1875–1883, DOI: [10.1021/acssensors.1c00139](https://doi.org/10.1021/acssensors.1c00139).
- 18 J.-M. Moon, H. Teymourian, E. De la Paz, J. R. Sempionatto, K. Mahato, T. Sonsa-ard, N. Huang, K. Longardner, I. Litvan and J. Wang, Non-Invasive Sweat-Based Tracking of L-Dopa Pharmacokinetic Profiles Following an Oral Tablet Administration, *Angew. Chem.*, 2021, **133**(35), 19222–19226, DOI: [10.1002/ange.202106674](https://doi.org/10.1002/ange.202106674).
- 19 M. Bariya, L. Li, R. Ghattamaneni, C. H. Ahn, H. Y. Y. Nyein, L.-C. Tai and A. Javey, Glove-Based Sensors for Multimodal Monitoring of Natural Sweat, *Sci. Adv.*, 2020, **6**(35), eabb8308, DOI: [10.1126/sciadv.abb8308](https://doi.org/10.1126/sciadv.abb8308).
- 20 S. Ding, T. Saha, L. Yin, R. Liu, M. I. Khan, A.-Y. Chang, H. Lee, H. Zhao, Y. Liu, A. S. Nazemi, J. Zhou, C. Chen, Z. Li, C. Zhang, S. Earney, S. Tang, O. Djassemi, X. Chen, M. Lin, S. S. Sandhu, J.-M. Moon, C. Moonla, P. Nandhakumar, Y. Park, K. Mahato, S. Xu and J. Wang, A Fingertip-Wearable Microgrid System for Autonomous Energy Management and Metabolic Monitoring, *Nat. Electron.*, 2024, **7**(9), 788–799, DOI: [10.1038/s41928-024-01236-7](https://doi.org/10.1038/s41928-024-01236-7).
- 21 T. Saha, M. I. Khan, S. S. Sandhu, L. Yin, S. Earney, C. Zhang, O. Djassemi, Z. Wang, J. Han, A. Abdal, S. Srivatsa, S. Ding and J. Wang, A Passive Perspiration Inspired Wearable Platform for Continuous Glucose Monitoring, *Adv. Sci.*, 2024, **24**05518, DOI: [10.1002/advs.202405518](https://doi.org/10.1002/advs.202405518).
- 22 J. T. Reeder, J. Choi, Y. Xue, P. Gutruf, J. Hanson, M. Liu, T. Ray, A. J. Bandodkar, R. Avila, W. Xia, S. Krishnan, S. Xu, K. Barnes, M. Pahnke, R. Ghaffari, Y. Huang and J. A. Rogers, Waterproof, Electronics-Enabled, Epidermal Microfluidic Devices for Sweat Collection, Biomarker Analysis, and Thermography in Aquatic Settings, *Sci. Adv.*, 2019, **5**(1), eaau6356, DOI: [10.1126/sciadv.aau6356](https://doi.org/10.1126/sciadv.aau6356).
- 23 J. C. Spinelli, B. J. Suleski, D. E. Wright, J. L. Grow, G. R. Fagans, M. J. Buckley, D. S. Yang, K. Yang, S. M. Beil, J. C. Wallace, T. S. DiZoglio, J. B. Model, S. Love, D. E. Macintosh, A. P. Scarth, M. T. Marrapode, C. Serviente, R. Avila, B. K. Alahmad, M. A. Busa, J. A. Wright, W. Li, D. J. Casa, J. A. Rogers, S. P. Lee, R. Ghaffari and A. J. Aranyosi, Wearable Microfluidic Biosensors with Haptic Feedback for Continuous Monitoring of Hydration Biomarkers in Workers, *NPJ Digit. Med.*, 2025, **8**(1), 1–12, DOI: [10.1038/s41746-025-01466-9](https://doi.org/10.1038/s41746-025-01466-9).
- 24 C. A. Machado-Moreira, J. N. Caldwell, I. B. Mekjavić and N. A. S. Taylor, Sweaty Hands: Differences in Sweat Secretion from Palmar and Dorsal Surfaces, in *Proceedings of the 12th International Conference on Environmental Ergonomics*, Piran Slovenia, 2007.
- 25 M. Bariya, N. Davis, L. Gillan, E. Jansson, A. Kokkonen, C. McCaffrey, J. Hiltunen and A. Javey, Resettable Microfluidics for Broad-Range and Prolonged Sweat Rate Sensing, *ACS Sens.*, 2022, **7**(4), 1156–1164, DOI: [10.1021/acssensors.2c00177](https://doi.org/10.1021/acssensors.2c00177).
- 26 M. Dautta, L. F. Ayala-Cardona, N. Davis, A. Aggarwal, J. Park, S. Wang, L. Gillan, E. Jansson, M. Hietala, H. Ko, J.

- Hiltunen and A. Javey, Tape-Free, Digital Wearable Band for Exercise Sweat Rate Monitoring, *Adv. Mater. Technol.*, 2023, 2201187, DOI: [10.1002/admt.202201187](https://doi.org/10.1002/admt.202201187).
- 27 N. Davis, A. Kang, E. Hakola, L. Gillan, Y. Zhan, J. Hiltunen and A. Javey, Reusable, Fully Integrated Sweat Monitor Band with Peel-and-Stick-Replacement Printed Microfluidic Sensor, *Adv. Mater. Technol.*, 2025, 2500477, DOI: [10.1002/admt.202500477](https://doi.org/10.1002/admt.202500477).
- 28 V. Laroy, F. Spaans and J. Reulen, The Sensory Innervation Pattern of the Fingers, *J. Neurol.*, 1998, 245(5), 294–298, DOI: [10.1007/s004150050221](https://doi.org/10.1007/s004150050221).